crystals

MDPI

Article

Effect of Aging State on the Microstructure and Tensile Properties of Al-7.0Zn-2.5Mg-2.0Cu-0.1Zr-0.2Sc Alloy

Xueyu Jiang [1,2], Xin Che [1,2,*], Mingxi Zhu [1,2] and Chunbo Liu [1,2]

[1] School of Materials Science and Engineering, Shenyang University of Technology, Shenyang 110870, China
[2] Shenyang Key Laboratory of Advanced Structural Materials and Applications, Shenyang University of Technology, Shenyang 110870, China
* Correspondence: xiaoxin2004068@163.com; Tel.: +86-177-0243-1616

Abstract: Tensile experiments were conducted for Al-7.0Zn-2.5Mg-2.0Cu-0.1Zr-0.2Sc alloy in different aging states (18 h, 24 h, 36 h) with temperature environments including room temperature, −10 °C and −30 °C. Comparative studies were made on the evolution of the precipitate phase in alloys at three kinds of aging times and the evolution of tensile properties in alloys under different ambient temperatures. The findings showed that the precipitates in Al-7.0Zn-2.5Mg-2.0Cu-0.1Zr-0.2Sc alloy were mainly in the GP zone after the solution + aging treatment η′ phase, the secondary Al_3 (Sc, Zr) phase and the θ′ (Al_2Cu) phase. As the aging time was prolonged, the η′ phase gradually grew and the PFZ gradually widened. At the three test temperatures, the tensile strength (TS) and yield strength (YS) of the alloys both showed a trend of first increasing before decreasing with the extension of aging time, while the elongation (A) and section shrinkage (Z) showed a decreasing trend. As the test temperature decreased, the TS and YS of the alloys increased and the A and Z of the alloys decreased. At room temperature, alloys showed a ductile fracture mode, which changed to mixed ductile and brittle fracture with decreasing test temperature.

Keywords: Al-Zn-Mg-Cu-Zr-Sc alloy; low temperature; tensile property; microstructure

Citation: Jiang, X.; Che, X.; Zhu, M.; Liu, C. Effect of Aging State on the Microstructure and Tensile Properties of Al-7.0Zn-2.5Mg-2.0Cu-0.1Zr-0.2Sc Alloy. *Crystals* **2023**, *13*, 581. https://doi.org/10.3390/cryst13040581

Academic Editors: Marek Sroka, Grzegorz Golański and Patrice Berthod

Received: 3 March 2023
Revised: 21 March 2023
Accepted: 22 March 2023
Published: 28 March 2023

1. Introduction

As structural materials, Al-Zn-Mg-Cu alloys are widely used in various fields—such as automobiles, ships, aerospace industry, and so on—because of their high plasticity and high corrosion resistance, as well as their good strength-to-weight ratio [1–3]. In industrial production, this series of alloys is usually produced through casting, powder metallurgy, spray forming, electromagnetic stirring, and other forming technologies. In the following experiment, micro-alloying, heat treatment and plastic processing are adopted to enhance the performance of this series of alloys [4–6]. Adding alloying elements is a critical factor in strengthening the properties of Al-Zn-Mg-Cu alloys, and the regulation of the species and proportions of the added alloying elements has been carried out throughout the alloys' development. The mechanical performance of alloys is strengthened by adjustments to the heat treatment process, which is essentially due to the lattice distortion caused by its elements or the second-phase formation within the matrix material [7,8]. At present, researchers have investigated this series of alloys from multiple angles, including by optimizing the design of new grades of alloys through further adjustments to the alloys' composition to fundamentally change their overall performance. It is also possible to improve the heat treatment process to affect the evolution of the alloy's microstructure, which then regulates the alloy to exhibit mechanical properties at the macroscopic level. First, the existing heat-treating procedure is further improved and optimized. In addition, a new heat treatment process that is more suitable for industrial production will be developed to explore more deeply the strengthening mechanism of aluminum alloys from the microscopic point of view, as well as to realize improvements in their macroscopic properties by controlling their microstructure [9,10].

Al-Zn-Mg-Cu alloys are heat-treatable strengthening alloys. After a solution treatment, this series of alloys will be desolventized in a low-temperature aging, and plenty of fine and dispersed particles such as the GP region and η′ will be precipitated. Because of the pinning effect of these strengthening phases, the dislocation movement of the alloys is hindered, and dispersion strengthening then occurs [11,12]. The over-saturated solid solution formed by this series of alloys is unstable after the solid solution, and the energy difference will promote its own decomposition. This is mainly due to the higher alloying degree of this serial alloy, so that the precipitation of the second-phase Tanlianker et al. [13] proposed a regression re-aging (RRA) treatment regime based on the T77 aging process, in the hope of achieving a balanced alloy synthesis by combining the advantages of single-stage and dual-stage aging. Regression re-aging (RRA) is divided into three main stages, the first of which is low-temperature pre-aging, a phase with a long holding time aimed at precipitating a large number of strengthening phases such as the GP zone and η′. The second stage is high-temperature regression aging, which means that the alloys are heated and kept warm for a short amount of time (the temperature range is between the pre-aging temperature and the solution temperature). In this process, small GP zones and η′ phase structures inside the grains decrease with volume fraction, while the η′ phase grows discretely around the grains' boundaries. A major breakthrough has also been made in the research on the regression re-aging process. Han et al. [14] found that the temperature of the regression treatment would affect the properties of 7050 aluminum alloy. When the regression temperature was of 150 °C and 170 °C, the alloy's strength and fracture toughness were improved. In addition, Xu et al. [15]'s research results achieved the best comprehensive properties when treating AA7150 aluminum alloy by slowly raising the temperature in the pre-aging stage and keeping the temperature at 65 °C.

Compared with the room-temperature environment, the microstructure of the tensile-deformation zone of alloys in the low-temperature environment often undergoes large changes and the fracture mechanism may also be different. Currently, the fatigue behavior of aluminum alloys is mostly studied under high-temperature, corrosion and high-circumference conditions, and the 2xxx series alloys are the most-studied subjects. In contrast, there is relatively little research on the low-temperature tensile behaviors of such alloys. In low-temperature environments, tensile fracture sometimes occurs more rapidly, with a shorter duration and no obvious signs before fracture. Therefore, the study of the tensile mechanisms in this series of alloys at low temperatures is indispensable for ensuring their practical and safe application and has important research value and practical significance.

2. Experiment

For the present experiment, the material used was Al-Zn-Mg-Cu-Zr-Sc alloy in the hot-extruded state, prepared from high-purity Al, pure Zn, pure Cu, pure Mg and Al-5%Zr and Al-2%Sc intermediate alloys. The specific chemical components and contents (wt.%) were 7.0Zn, 2.5Mg, 2.0Cu, 0.1Zr, 0.2Sc, Bal.Al by ARL PERFORM′X fluorescence spectrometer composition analysis. After homogenization treatment (460 °C × 24 h + air cooling), hot extrusion was performed using a 1250 t horizontal extruder at 460 °C preheating temperature, 490 °C extrusion temperature, 2.5 mm/s extrusion speed and 20:1 extrusion ratio.

Al-7.0Zn-2.5Mg-2.0Cu-0.1Zr-0.2Sc alloy was treated by solid solution + single-stage aging using JHF-27 heat treatment furnace. The solid-solution-treatment process was 475 °C × 2 h + water quenching. The aging temperature was 110 °C for 18 h, 24 h, 36 h, and air cooling. The tensile properties of the different aging states of alloys were tested using a WDW-200E microcomputer-controlled electronic universal testing machine. The alloy specimens were subjected to tensile tests under the following temperature environments: room temperature, −10 °C and −30 °C. When the experiment was conducted in low-temperature environment, the specimen was pre-insulated for approximately 20 min, and the tensile rate was set to 2 mm/min. Tensile specimens and dimensions are shown in Figure 1.

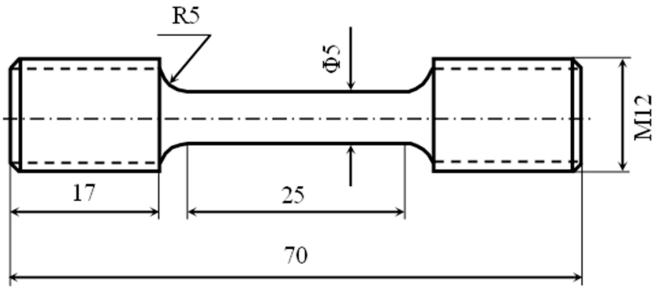

Figure 1. Tensile specimen and size.

Microstructure in alloys during the second phase was observed by JEM-2100 transmission electron microscope. The transmission samples were thinned using a Tenupol-5 double-spray thinner with a double-spray electrolyte of 25 wt.% HNO_3 + 75 wt.% CH_3OH solution. Before starting the sample preparation, the temperature of the electrolyte was reduced to approximately −30 °C., the operating voltage of the equipment was set to approximately 17 V, and the operating current was controlled at approximately 80 mA. The tensile fracture of alloy samples was observed and analyzed using an S3400N scanning electron microscope.

3. Results

3.1. Microstructure Analysis

Figure 2 shows the metallographic structure of the experimental alloy when aged at 110 °C at different times. As shown in the Figure, there was little difference in grain size when Al-7.0Zn-2.5Mg-2.0Cu-0.1Zr-0.2Sc alloy was under the solid solution + aging treatment.

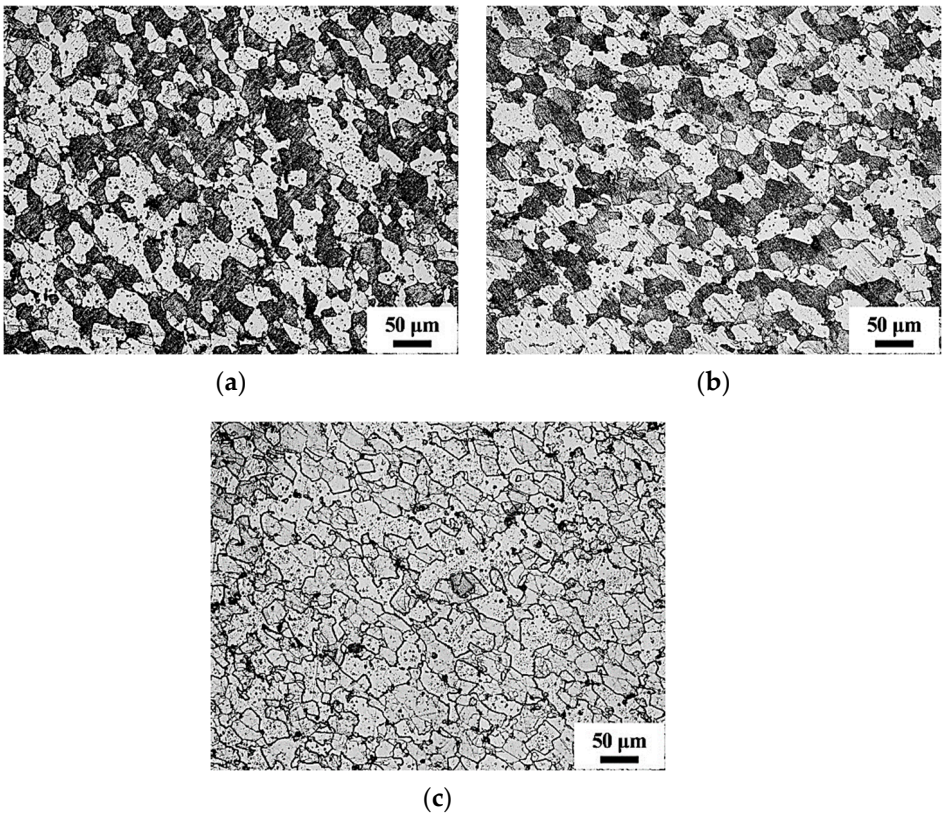

(**a**) (**b**)

(**c**)

Figure 2. Metallography of alloy at different aging times: (**a**) solution + aging 18 h; (**b**) solution + aging 24 h; (**c**) solution + aging 36 h.

The TEM photographs of the solid solution + aging state of Al-7.0Zn-2.5Mg-2.0Cu-0.1Zr-0.2Sc alloy were shown in Figure 3. From Figure 3a,c,e, it can be observed that a great number of bean-like precipitated phases were found spread in the substrate of the alloys at different aging times. Combining the diffraction maps in Figure 3b,d,f and the related literature [16], it was clear that this bean-like second phase was the secondary Al_3(Sc, Zr) phase, and $1/2\{220\}_{Al}$ was the site where its derivative point appeared. Meanwhile, a non-serif band was detected on the particles of the secondary Al_3(Sc, Zr) phase, and the presence of the non-serif band showed that the secondary Al_3(Sc, Zr) phase had a nice co-localization with the Al substrate. As seen in Figure 3b,d,f, the alloys at different aging times were distributed with finer second phases than the secondary Al_3(Sc, Zr) phases, which were numerous and uniformly diffuse in the α-Al matrix. Combining the electron diffraction pattern in the figure and the related literature [17], it was clear that the fine-grained phases appearing in the TEM images were the GP region and the η′ phase. The η′ phase appeared at $1/3\{220\}_{Al,}$ or $2/3\{220\}_{Al}$ in the SAED pattern, while the GP region corresponded to $1/4\{430\}_{Al}$ in the SAED pattern. In Figure 3b, after aging for 18 h, both the GP zone and the η′ phase were found within the alloy. In Figure 3d, after having increased the aging time to 24 h, the diffraction bright spot in the η′ phase was still present in the electron diffraction pattern. However, the diffraction bright spot in the GP zone was not as obvious as it was when under 18h of aging, and was relatively dark, indicating that more of the GP zone had been converted into the η′ phase. From Figure 3d, one could see that the apparent growth of the η′ phase occurred during an aging time of between 24 h and 36 h.

In addition to the secondary Al_3(Sc, Zr) phase, the GP zone and the η′ phase, another secondary phase was found in the T6 state alloy, and the morphology of this phase under TEM and the electron diffraction pattern of the corresponding selected region are shown in Figure 4a. This phase had a sub-circular appearance with a diameter of approximately 120 nm. The results of the EDS analysis of this phase are shown in Figure 4b, while the mass percentages and chemical atomic ratios of the chemical elements composing this phase are listed in Table 1. As can be seen from Figure 4b, the major elements forming this phase were Al, Cu, and minor amounts of Zn, Mg and Sc. From Table 1, it can be observed that the proportion of Al and Cu atoms in this phase was close to 2:1; combined with the derivative patterns and related papers, the phase was determined to be a θ′(Al_2Cu) phase [18].

Table 1. EDS analysis results of precipitated phase in alloy.

Element	Al	Zn	Mg	Cu	Sc
wt.%	36.23	6.94	0.55	49.91	6.37
at.%	55.97	4.42	0.94	32.75	5.91

The TEM bright-field images for Al-7.0Zn-2.5Mg-2.0Cu-0.1Zr-0.2Sc alloy located at the grain boundary and in its vicinity are illustrated in Figure 5. As can be seen in the Figure, after the solid solution + aging treatment, there were precipitation-free zones (PFZ) surrounding all the grain boundaries, while the precipitation phase (GBP) was present at the grain boundaries. As seen in Figure 5a, when the aging time was 18 h, the GBP was chain-like, with a uniform, continuous arrangement at the grain boundaries and a PFZ's width of approximately 14.8 nm. Upon increasing the aging time to 24 h, the size of the GBP increased and was intermittently arranged at the grain boundaries, and the PFZ's width increased to 18.7 nm, as illustrated in Figure 5b. Following the 36h aging treatment, the GBP's size and the PFZ's width continually grew, with the PFZ's width reaching 21.3 nm, as illustrated in Figure 5c.

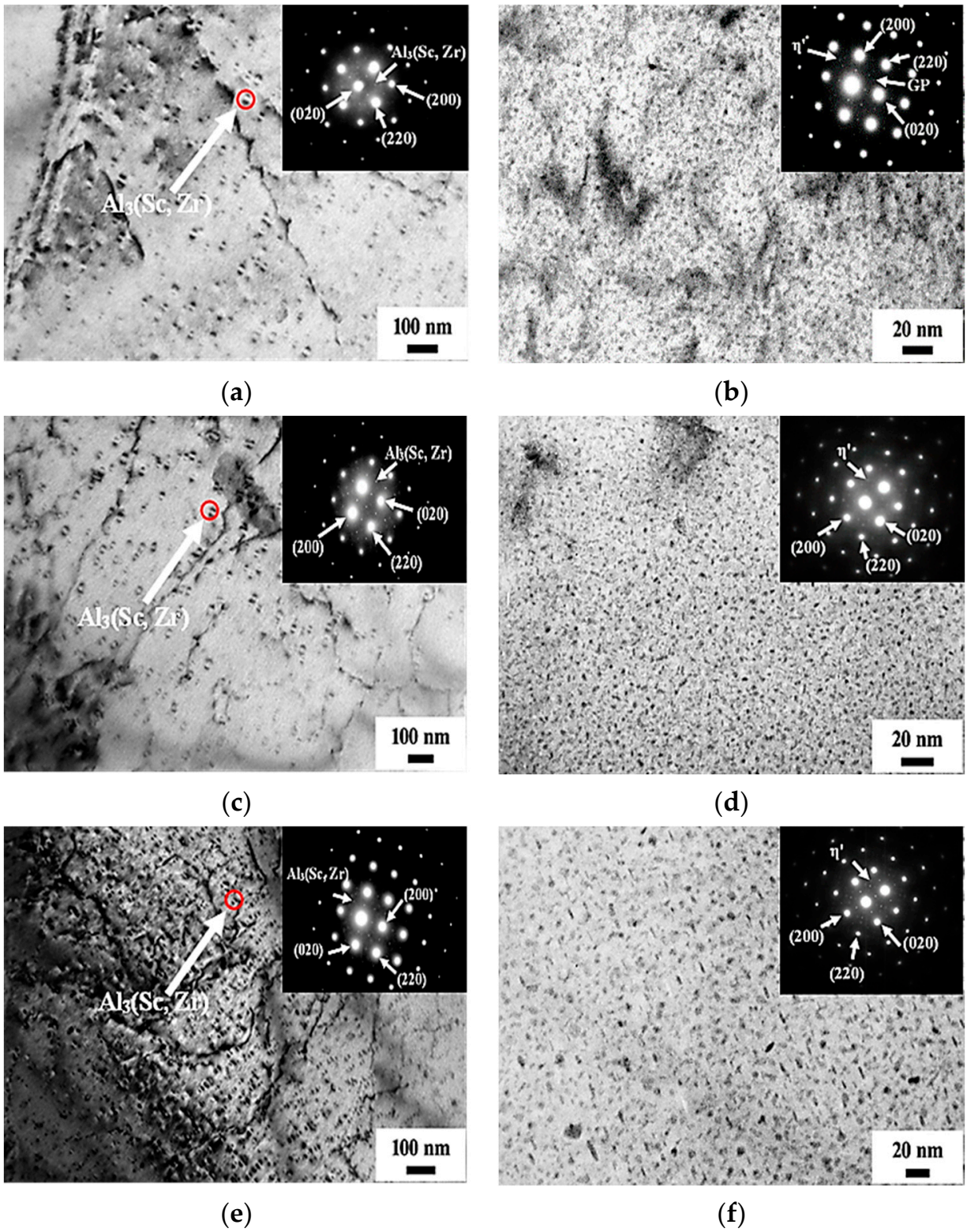

Figure 3. Morphology and electron diffraction pattern of precipitated phase in T6 alloy. (**a**,**b**) Solution + aging 18 h; (**c**,**d**) solution + aging 24 h; (**e**,**f**) solution + aging 36 h.

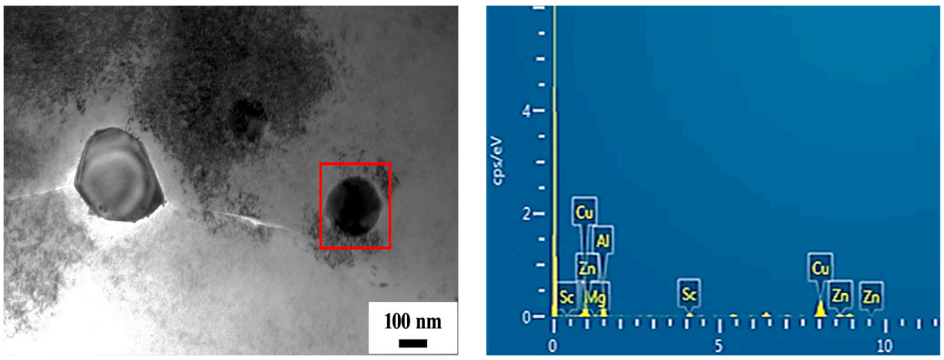

(**a**) (**b**)

Figure 4. Morphology and energy spectrum analysis of precipitated phase in T6 alloy.

3.2. Tensile Properties

3.2.1. Tensile Curves of Alloys

The tensile properties of Al-7.0Zn-2.5Mg-2.0Cu-0.1Zr-0.2Sc alloy were affected by both aging time and experimental temperature, and they tended to change significantly when the alloys underwent different aging times and were at different ambient temperatures. Figure 6a presents the curves of TS versus aging time for this alloy at various experimental temperatures. As shown in the Figure, the TS of the alloy exhibited a rising and then declining trend with increases in aging time, both at room temperature and low temperature. Moreover, for the same aging time, the decrease in ambient temperature led to a gradual increase in the TS of the alloy [19]. After 24 h of aging, the TS of the alloy reached a peak value in both room-temperature and low-temperature environments, with a maximum TS of 650 MPa at room temperature, 659 MPa at −10 °C, and an increase to 670 MPa at −30 °C. The YS versus aging time curves of the alloy in room-temperature and low-temperature environments are illustrated in Figure 6b. As shown in the Figure, the YS of Al-7.0Zn-2.5Mg-2.0Cu-0.1Zr-0.2Sc alloy exhibited a similar trend to that of the TS at different experimental temperatures, increasing and then decreasing with aging time, and reaching a peak at 24 h of aging. The YS of the alloy at identical aging times differed when the ambient temperature varied. Comparing the YS of the alloy at identical aging times, it was observed that the YS gradually improved as decreased. At room temperature, the maximum YS of this alloy was 591 MPa., 602 MPa at −10 °C-temperature environment, and 612 MPa at −30 °C-temperature environment. The curves of post-break elongation versus aging time for Al-7.0Zn-2.5Mg-2.0Cu-0.1Zr-0.2Sc alloy at room temperature and low temperature are shown in Figure 6c. It can be seen from the Figure that the post-extension after aging time tended to decrease for the alloy at different experimental temperatures. Comparing the elongation at break of alloys with the same aging time, it can be seen that the elongation at break of alloys with the same aging time showed a decreasing trend when the experimental temperature decreased. Figure 6d shows the surface shrinkage of Al-7.0Zn-2.5Mg-2.0Cu-0.1Zr-0.2Sc alloy at various experimental temperatures as a function of aging time. The Figure shows that the effect of aging time and experimental temperature on the cross-sectional contraction rate of Al-7.0Zn-2.5Mg-2.0Cu-0.1Zr-0.2Sc alloy was comparable to the influence of stretching after fracture. The section elongation of the alloy showed a decreasing trend with increasing aging time at room temperature and low temperature, while the section shrinkage of the alloy decreased with decreasing experimental temperature at the same aging times.

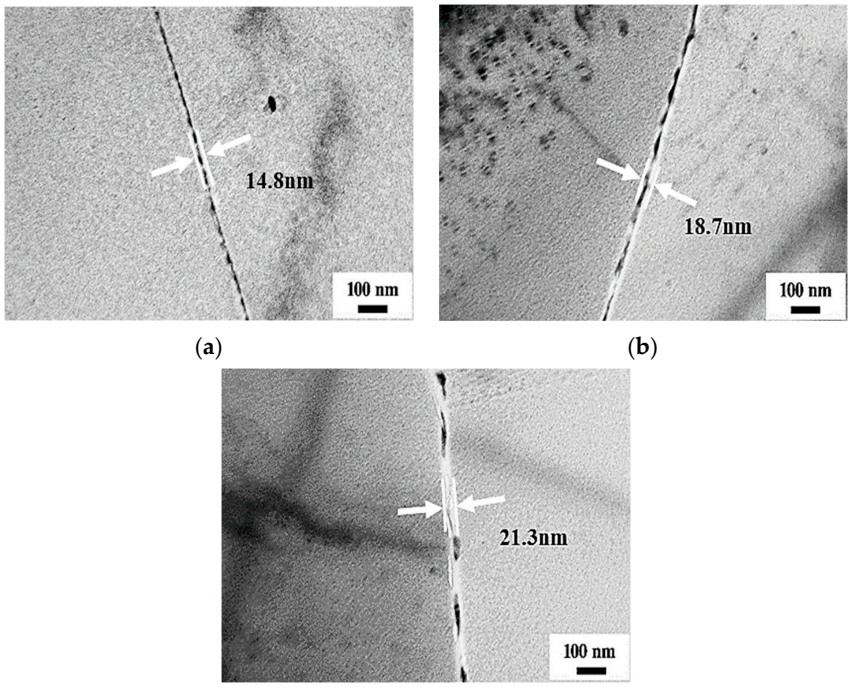

Figure 5. Grain boundary morphology of T6 alloy: (**a**) solution + aging 18 h; (**b**) solution + aging 24 h; (**c**) solution + aging 36 h.

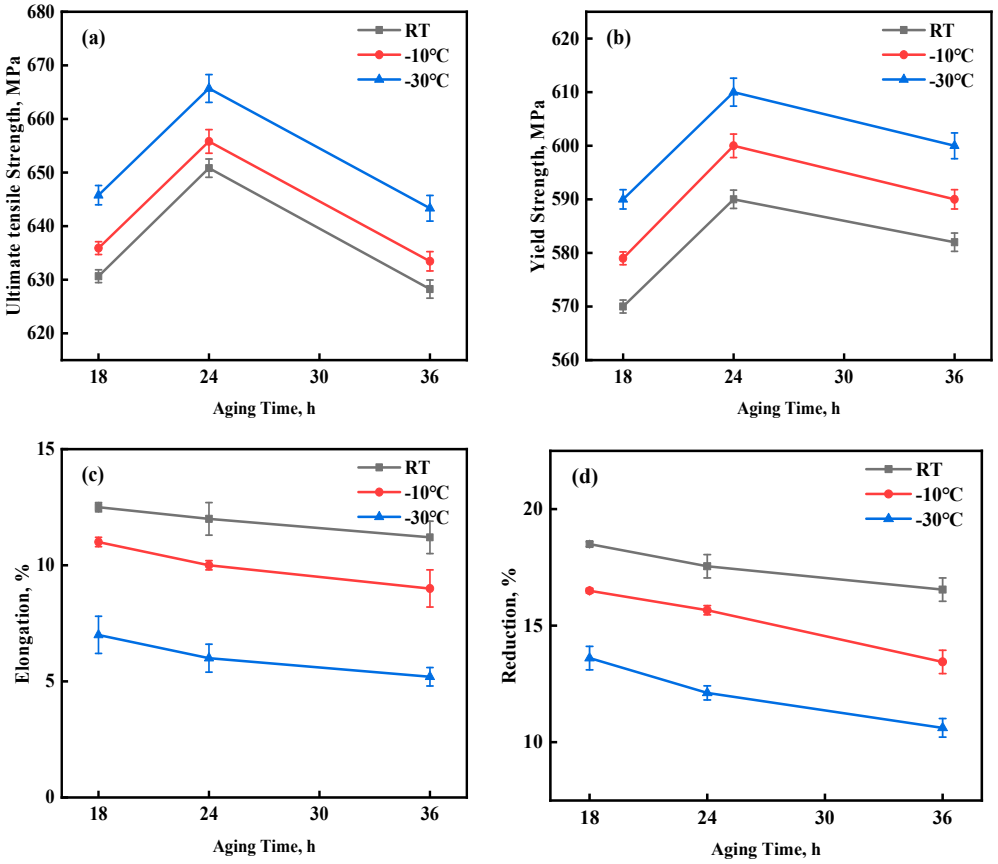

Figure 6. Mechanical properties of alloys at different experimental temperatures: (**a**) TS versus aging time; (**b**) YS versus aging time; (**c**) elongation after fracture versus aging time; (**d**) reduction after fracture versus aging time.

3.2.2. Tensile Fracture Morphology

The tensile fracture of the alloy was viewed by an SEM to identify the alloy's mechanism of fracture under different application conditions. The tensile fracture pattern of Al-7.0Zn-2.5Mg-2.0Cu-0.1Zr-0.2Sc alloy in the solid solution + aging state at room-temperature environment is illustrated in Figure 7. As seen in the Figure, when the applied experimental temperature was room temperature, many tough nests and tear ribs appeared on the alloy's tensile fracture surface. With the increase in aging time, the number of tough nests on the alloy's tensile fracture surface decreased significantly, and their size and depth also decreased, which corresponds to the decreasing trend in the alloy's post-extension and section shrinkage when aging time increases. The above phenomena indicate that the fracture mode of the solid solution + aging state of Al-7.0Zn-2.5Mg-2.0Cu-0.1Zr-0.2Sc alloy was ductile fracture in a room-temperature environment.

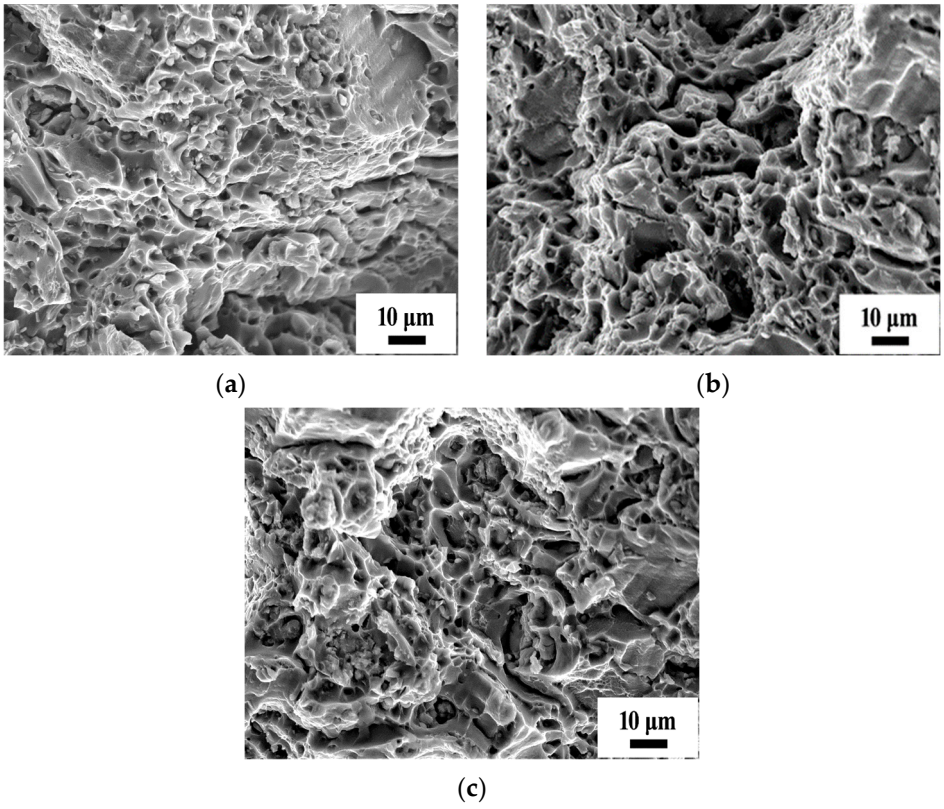

Figure 7. Tensile fracture morphology of alloys in solid solution + aging at room temperature: (**a**) solution + aging 18 h; (**b**) solution + aging 24 h; (**c**) solution + aging 36 h.

Figure 8 displays the tensile fracture surface morphology of Al-7.0Zn-2.5Mg-2.0Cu-0.1Zr-0.2Sc alloy in the solid solution + aging condition at a low temperature of −10 °C. As can be seen from the Figure, at the experimental temperature of −10 °C, there were still dimples and tear edges on the tensile fracture surface of Al-7.0Zn-2.5Mg-2.0Cu-0.1Zr-0.2Sc alloy, but there were also a certain number of cleavage facets. At that time, the alloy exhibited a fracture characteristic of mixed toughness and brittleness. The above observations indicate that the increase in aging time and the decrease in experimental temperature both decrease the plasticity of Al-7.0Zn-2.5Mg-2.0Cu-0.1Zr-0.2Sc alloy.

Figure 9 presents the tensile fracture topography of Al-7.0Zn-2.5Mg-2.0Cu-0.1Zr-0.2Sc alloy at a low temperature of −30 °C. As can be seen from the Figure, when the experimental temperature was −30 °C, the number of ductile fracture features such as dimples and tear edges on the tensile fracture surface of the alloy significantly decreased. The proportion of cleavage facets on the fracture surface significantly increased, and the tensile fracture exhibited a typical ductile–brittle mixed fracture. The above phenomena indicated that the

brittle fracture tendency of the alloy was more pronounced with further decreases in the experimental temperature.

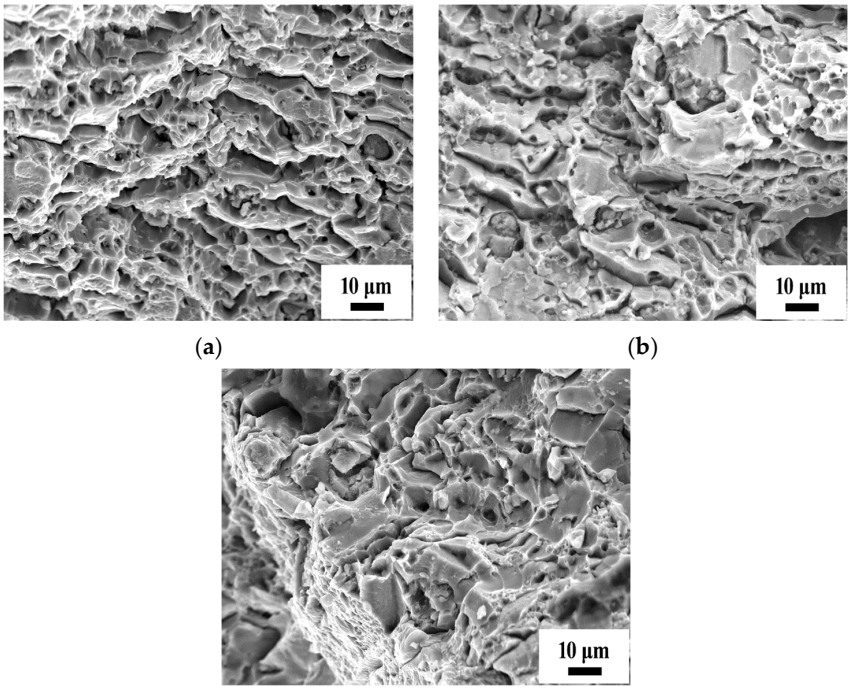

(**a**) (**b**)

(**c**)

Figure 8. Tensile fracture morphology of alloys in solid solution + aging at −10 °C: (**a**) solution + aging 18 h; (**b**) solution + aging 24 h; (**c**) solution + aging 36 h.

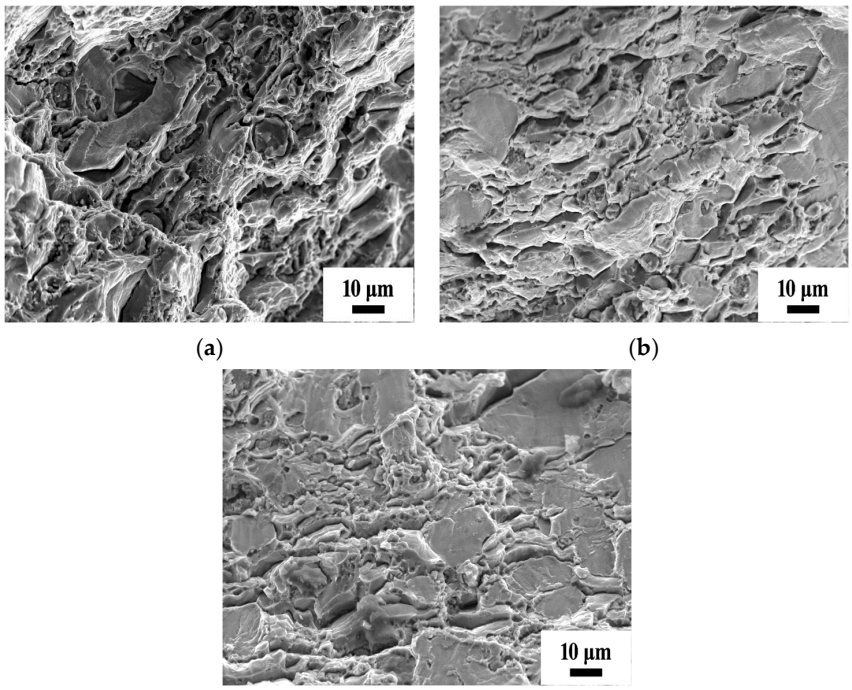

(**a**) (**b**)

(**c**)

Figure 9. Tensile fracture morphology of the alloy in solid solution + aging at −30 °C: (**a**) solution + aging 18 h; (**b**) solution + aging 24 h; (**c**) solution + aging 36 h.

4. Discussion

After Al-7.0Zn-2.5Mg-2.0Cu-0.1Zr-0.2Sc was melted and cast, elemental segregation created many non-equilibrium eutectic phases within the alloy that caused the deterioration of its properties, and homogenization was an effective means of eliminating composition segregation [19–21]. After homogenization, the segregated alloying elements and the coarse non-stationary phases within the alloy underwent re-solution to equilibrate the properties of the as-cast alloy, improve its plasticity during thermal deformation and reduce the risk of extrusion cracking during subsequent hot extrusions. After the heat treatment process of the solid solution at 475 °C + 110 °C aging, the grain size of Al-7.0Zn-2.5Mg-2.0Cu-0.1Zr-0.2Sc alloy did not show significant growth. The precipitated phases in the alloy consisted mainly of an Al_3(Sc, Zr) phase, an η′ ($MgZn_2$) phase, and a θ′(Al_2Cu) phase. The η′($MgZn_2$) phase has a high melting point and superior thermal-stability properties and can be used as a heterogeneous core for nucleation during the casting process, significantly improving the alloy nucleation rate and thus refining Al-7.0 Zn-2.5Mg-2.0Cu-0.1Zr-0.2Sc alloy. The η′($MgZn_2$) phase is diffusely spread in the Al matrix, which for Al-7.0Zn-2.5Mg-2.0Cu-0.1Zr-0.2Sc alloy [20]. At some temperatures, it can also solid-solve in the aluminum phases in aging, thus greatly improving the mechanical properties of the alloy. After the solid-solution treatment, most of the second phase in Al-7.0Zn-2.5Mg-2.0Cu-0.1Zr-0.2Sc alloy is dissolved into the matrix and precipitated in the aging stage. Secondary Al_3(Sc, Zr) phases were found within the Al matrix at different aging times, and it has been suggested [16] that the dislocations and subgrain borders present in this phase produce a rather strong pinning effect, thus offering various strength-enhancing effects in the alloy. Since the secondary Al_3(Sc, Zr) phase fixes dislocations and impedes the migration of grain boundaries, the recrystallization temperature of Al-7.0Zn-2.5Mg-2.0Cu-0.1Zr-0.2Sc alloy is greatly enhanced and a large number of dislocations and fine subgrain organization can be preserved in the solid solution + age-treated alloy, which is extremely advantageous for enhancing the tensile properties of the alloy.

Besides the secondary Al_3(Sc, Zr) phase, the GP zone and the η′ phase were resolved in the solid solution + aging-treated alloy, and the presence of these two was the most significant reason for the greatly increased tensile properties of the Al-Zn-Mg-Cu-system alloy, which was also the underlying purpose of adding Zn and Mg elements. The relevant literature [20] has clarified that the phase-precipitation sequence in 7xxx-series aluminum alloys was SSS (supersaturated solid solution) → GP zone → η′ phase ($MgZn_2$) → η phase ($MgZn_2$). As the alloys in this paper were aged at a constant temperature of 110 °C, the primary factor affecting the order of the alloy's strengthening-phase precipitation is the aging time. At an aging temperature of 110 °C, the aging time influences the morphology, size and distribution of the intracrystalline phase (MPt) of Al-7.0Zn-2.5Mg-2.0Cu-0.1Zr-0.2Sc alloy, in combination with the morphology and distribution of the grain-boundary-free zone (PFZ) and the grain-boundary-precipitation phase (GBP). There are two explanations for the formation of PFZs: one is the atom-poor theory. The grain boundary, as the place where vacancies are concentrated in the alloy, is usually in a higher energy state, and alloy atoms tend to accumulate towards the grain boundary and thus form second-phase particles. This phenomenon results in a decrease in the number of alloy atoms near the grain boundaries, creating a scarcity of alloy atoms—especially Zn atoms—near the grain boundaries, thus making the formation of a second phase near the grain boundaries insufficient, which leads to the formation of a precipitation-free zone (PFZ) around the grain boundaries. Another explanation is the critical-vacancy theory. This theory suggests that the second phase needs to be formed at a certain concentration of vacancies, and most of the vacancies near the grain boundaries slip into the intergranular area, making the concentration of vacancies in the vicinity lower than the critical vacancy concentration needed for the formation of the second phase. In addition to the second phase mentioned above, another nano-phase was found in the solid solution + aging-treated alloy, which was identified by diffraction patterns as the θ′(Al_2Cu) phase [21]. From the above analysis, it is clear that the element Cu can also form precipitation-reinforced phases of relatively

small sizes, in addition to forming solid solutions in Al-7.0Zn-2.5Mg-2.0Cu-0.1Zr-0.2Sc alloy or coarser eutectic phases.

The tensile test results indicated that the tensile properties of the solid solution + aging-treated Al-7.0Zn-2.5Mg-2.0Cu-0.1Zr-0.2Sc alloy were affected by both the aging time and the ambient temperature. The strength and plasticity of the alloys at the same experimental temperature and the trend of the aging time are closely correlated with the changes in the microstructure of the alloys. Since the heat treatment has little influence on the grain size and grain-boundary-disorientation of the alloy, the tensile properties of the alloy are mainly defined by the precipitated phases during aging. The order of precipitation and the appearance of the second phase in the alloy are closely linked to the aging time, as shown in the previous section. In the initial stage of aging, the alloying elements (mainly Mg and Zn elements) dissolved in the matrix undergo segregation in the supersaturated solid solution to produce GP zones, and as more and more GP zones precipitate in the Al matrix, they form an obstruction in the dislocations' path of movement, causing an initial increase in the strength of the alloy. At the mid-aging stage, the GP zone transforms into the η′ phase, which is semi-coherent with the matrix and plays a serious interference role in the dislocation motion, so the appearance of the η′ phase leads to another increase in the TS of the alloy. When most of the GP region in the alloy is transformed into the η′ phase, the interaction between the dislocation and the second phase is at the critical stage of transformation from a cut-through into a bypass mechanism and, at this time, the TS of the alloy increases to its peak. As the aging time continues to increase, the η′ phase in the alloy begins to coarsen and transforms into the η phase [22]. The co-grid relationship with the matrix also worsens, weakening the hindering effect on dislocations and decreasing the tensile and YS of the alloy. The decreases in the post-extension and section shrinkage of the alloy after fracture due to the increase in aging time could be explained by the morphological changes of the GBP and the PFZ. As the aging time increases, the GBP increases further, while the PFZ, which has fewer mechanical properties, also appears near the grain boundaries and gradually enlarges, which results in more severe stress concentration and property degradation at the grain boundaries and further degradation of the metal's plasticity [23–25]. The tendency of the strength and plasticity of the alloy to rise with temperature when the aging time is the same may be related to the strength of the atomic motion ability. In the room-temperature environment, the interaction between dislocations and precipitated phases is weak, and dislocations can break free from the pegging of the second phase to slide out of the grain and move to the grain boundaries when the short-range resistance to the dislocation motion is weak and dislocations have a large movable space. As the temperature decreases, the thermal vibration and diffusion rate of the atoms in the alloy begin to weaken. At this time, the dislocations form cutting steps and the resistance to the movement of the cutting steps themselves increases, the obstruction of the second relative dislocation also increases under the influence of the combined factors, and the movable capacity of the dislocations decreases resulting in an increase in the alloy's TS and YS.

The tensile fracture morphology of Al-7.0Zn-2.5Mg-2.0Cu-0.1Zr-0.2Sc alloy at different experimental temperatures and aging times was observed, and it was found that when the experimental temperature was room temperature, the tensile fracture surface was distributed with many tough nests of different sizes and accompanied by some tearing-rib features. From the above, it is clear that the fracture mechanism of Al-7.0Zn-2.5Mg-2.0Cu-0.1Zr-0.2Sc alloy in room-temperature environment is ductile fracture. Residues of the second phase were found in the toughness nest, and according to the results of the energy spectral analysis, the elemental composition was found to be close to that of the Al_7Cu_2Fe phase and the S phase, which were directly responsible for the generation of the toughness-nest characteristics. The second-phase grains are different from the aluminum substrates during the tensile process of the sample due to the elastic modulus, so the degree of deformation is also very different, and it is easy to produce separation at the bond with the matrix. Moreover, the more brittle second phase itself can also easily produce stress concen-

tration when reaches a critical value, which will generate microcracks in the second phase or in the bond between the second phase and the substrate; as the degree of deformation increases, the microcracks will extend outward and interconnect, forming a tough nest, and some second-phase particles will be left at the base of the tough nest [25–28]. The results of the above analysis indicate that the coarse-eutectic phase can have a significant effect on the fracture behavior of the alloy. The number, size and depth of the fracture surfaces of Al-7.0Zn-2.5Mg-2.0Cu-0.1Zr-0.2Sc alloy declined as the experimental temperature decreased. The lower the experimental temperature, the smaller the proportion of tough nests on the fracture surface and the larger the proportion of destructive surfaces. The fracture mechanism of Al-7.0Zn-2.5Mg-2.0Cu-0.1Zr-0.2Sc alloy at experimental temperatures of −10 °C and −30 °C can be judged as a mixed tough–brittle fracture based on the morphological characteristics presented on the fracture surface. The toughness of Al-7.0Zn-2.5Mg-2.0Cu-0.1Zr-0.2Sc alloy decreases with the experimental temperature and aging time decreases with decreasing experimental temperature and aging time, which can also be explained by the motion of dislocations. When the external temperature decreases, the thermal-oscillation ability of the alloy atoms becomes weaker and the Pena force of the dislocation motion increases, which leads to the appearance of more dense slip bands during their slip—which are the preferred path for crack expansion—and consequently the formation of deconvolution facets on the fracture surface. Secondly, as the temperature decreases, specific contractions occur in the aluminum matrix and in a second phase distributed at the grain boundary. However, the degree of shrinkage is different, so microcracks are easily generated at the phase boundary, and the microcrack extension is connected to the formation of deconvolution facets [29,30]. With the prolongation of aging time, the width of the PFZ increases, which makes it easy for the grain boundary of Al-7.0 Zn-2.5 Mg-2.0 Cu-0.1 Zr-0.2 SC alloy and its vicinity to become a mechanical weak zone, where cracks tend to expand rapidly. Based on the above discussion, decreases in temperature and increases in aging time lead to the decrease in plasticity of Al-7.0Zn-2.5Mg-2.0Cu-0.1Zr-0.2Sc alloy.

5. Conclusions

(1) After the T6 treatment, the precipitated phases in Al-7.0Zn-2.5Mg-2.0Cu-0.1Zr-0.2Sc alloy mainly consisted of the GP region, the η′ phase, the secondary Al_3(Sc, Zr) phase, the θ′(Al_2Cu) phase, and the α-Al phase. With the extension of aging time, the η′ phase obviously increased. The precipitates at the grain boundary changed from having a continuous distribution to an interval distribution, and the width of the precipitate-free zone at the grain boundary gradually increased from 14.8 nm to 21.3 nm.

(2) The tensile and YSs of the T6 state Al-7.0Zn-2.5Mg-2.0Cu-0.1Zr-0.2Sc alloy at room temperature, −10 °C and −30 °C reached their maximum values at an aging time of 24h. At all three aging times, the TS and YS of the alloys increased with decreases in test temperature, and the elongation at break and shrinkage at section decreased with decreases in test temperature.

(3) The tensile fracture morphology of the T6 state Al-7.0Zn-2.5Mg-2.0Cu-0.1Zr-0.2Sc alloy at room temperature is characterized by tough nests and tearing ribs, and the fracture mechanism is ductile fracture. At −10 °C and −30 °C, the tensile fracture profile was characterized by the deconvolution facets and the fracture mechanism changed to mixed tough–brittle fracture.

In this paper, the tensile properties of Al-7.0Zn-2.5Mg-2.0Cu-0.1Zr-0.2Sc alloy under different conditions were tested at room temperature, −10 °C, and −30 °C. However, in practical engineering applications, it is still necessary to consider the impact of other factors under service conditions.

Author Contributions: Conceptualization, X.J. and X.C.; methodology, M.Z.; software, C.L.; writing—original draft preparation, X.J.; writing—review and editing, X.J. All authors have read and agreed to the published version of the manuscript.

Funding: This research received no external funding.

Informed Consent Statement: Informed consent was obtained from all subjects involved in the study.

Data Availability Statement: Data available in a publicly accessible repository.

Conflicts of Interest: The authors declare no conflict of interest.

References

1. Abd El-Aty, A.; Xu, Y.; Guo, X.; Zhang, S.H.; Ma, Y.; Chen, D. Strengthening mechanisms, deformation behavior, and anisotropic mechanical properties of Al-Li alloys: A review. *J. Adv. Res.* **2018**, *10*, 49–67. [CrossRef] [PubMed]
2. Zhang, Y.; Yang, L.; Fan, Z.; Pang, S.; Chen, W. Evaluation of tensile creep behavior of spray formed and extruded 7075 aluminum alloy by equivalent stress. *J. Mater. Res. Technol.* **2023**, *22*, 1476–1490. [CrossRef]
3. Yuan, M.; Wu, J.; Meng, Q.; Zhang, C.; Mao, X.; Huang, S.; Wang, S. The Role of Al_4C_3 Morphology in Tensile Properties of Carbon Fiber Reinforced 2024 Aluminum Alloy during Thermal Exposure. *Materials* **2022**, *15*, 8828. [CrossRef] [PubMed]
4. Bhat, R.S.; Manjunatha, K.B.; Prasanna Shankara, R.; Venkatakrishna, K.; Hegde, A.C. Electrochemical studies on the corrosion resistance of Zn–Ni–Co coating from acid chloride bath. *Appl. Phys. A* **2020**, *126*, 03958. [CrossRef]
5. Hao, Z.; Fu, X.; Men, X.; Zhou, B. Study on tensile and fracture properties of 7050-T7451 aluminum alloy based on material forming texture characteristics. *Mater. Res. Express* **2019**, *6*, 036502. [CrossRef]
6. Paul, A. Role of surface treatment and coating on tensile response and fracture behavior of aluminum alloy 7075. *Emerg. Mater. Res.* **2017**, *6*, 100–107.
7. Bhat, R.S.; Nagaraj, P.; Priyadarshini, S. Zn–Ni compositionally modulated multilayered alloy coatings for improved corrosion resistance. *Surf. Eng.* **2021**, *37*, 755–763. [CrossRef]
8. Xia, P.; Wang, S.; Huang, H.; Zhou, N.; Song, D.; Jia, Y. Effect of Sc and Zr additions on recrystallization behavior and intergranular corrosion resistance of Al-Zn-Mg-Cu alloys. *Materials* **2021**, *14*, 5516. [CrossRef]
9. Ma, J.; Wang, Q.; Zhang, T.Y. Effect of natural aging time on tensile and fatigue anisotropy of extruded 7075 Al alloy. *J. Mater. Res. Technol.* **2022**, *18*, 4683–4697. [CrossRef]
10. Zhang, Z.; Ma, X.; Zhang, C.; Chu, G.; Meng, Z.; Zhao, G.; Chen, L. Effect of stress-aging treatment on the mechanical and corrosion properties of Al− Zn− Mg− Cu alloy. *Mater. Sci. Eng. A* **2022**, *838*, 142791. [CrossRef]
11. Li, G.R.; Cheng, J.F.; Wang, H.M.; Li, P.S.; Li, C.Q. Influence of a high pulsed magnetic field on the tensile properties and phase transition of 7055 aluminum alloy. *Mater. Res. Express* **2016**, *3*, 106507. [CrossRef]
12. Dæhli, L.E.B.; Børvik, T.; Hopperstad, O.S. Influence of loading path on ductile fracture of tensile specimens made from aluminium alloys. *Int. J. Solids Struct.* **2016**, *88–89*, 17–34. [CrossRef]
13. Tanlianker, M.; Cina, B.M. Retrogression and reaging and the role of dislocations in the stress corrosion of 7000-type aluminum alloys. *Metall. Trans. A* **2020**, *20*, 2087–2092. [CrossRef]
14. Han, N.M.; Zhang, X.M.; Liu, S.D.; Huang, L.Y.; Xin, X.; He, D.G. Effects of retrogression and reaging on strength and fracture toughness of aluminum alloy 7050. *Chin. J. Nonferrous Met.* **2012**, *22*, 1871–1882.
15. Xu, D.K.; Birbilis, N.; Rometsch, P.A. The effect of pre-ageing temperature and retrogression heating rate on the strength and corrosion behaviour of AA7150. *Corros. Sci.* **2012**, *54*, 17–25. [CrossRef]
16. Wang, Y.; Li, Z.; Xiong, B.; Wen, K.; Huang, S.; Li, X.; Zhang, Y. Microstructure Evolution of High-Alloyed Al-Zn-Mg-Cu-Zr Alloy Containing Trace Amount of Sc During Homogenization. *Met. Mater. Int.* **2019**, *25*, 697–704. [CrossRef]
17. Lin, Y.C.; Zhang, J.L.; Liu, G.; Liang, Y.J. Effects of pre-treatments on aging precipitates and corrosion resistance of a creep-aged Al-Zn-Mg-Cu alloy. *Mater. Des.* **2015**, *83*, 866–875. [CrossRef]
18. Ma, X.G.; Li, S.Y.; Han, B.S.; Ye, F.; Rong, G.; Xu, Y.J.; Zeng, Y.S. Effect of pre-stretch on microstructure and properties of 2195 Al-Li alloy prepared by spray forming. *Chin. J. Nonferrous Met.* **2022**, *32*, 15–26.
19. Rao, A.U.; Vasu, V.; Govindaraju, M.; Srinadh, K.S. Stress corrosion cracking behaviour of 7xxx aluminum alloys: A literature review. *Trans. Nonferrous Met. Soc. China* **2016**, *26*, 1447–1471. [CrossRef]
20. Zhang, P.; Li, Z.M.; Liu, B. Tensile Properties and Deformation Behaviors of a New Aluminum Alloy for High Pressure Die Casting. *J. Mater. Sci. Technol.* **2016**, *33*, 367–378. [CrossRef]
21. Zou, Y.; Wu, X.; Tang, S.; Zhu, Q.; Song, H.; Guo, M.; Cao, L. Investigation on microstructure and mechanical properties of Al-Zn-Mg-Cu alloys with various Zn/Mg ratios. *J. Mater. Sci. Technol.* **2021**, *85*, 106–117. [CrossRef]
22. Li, H.; Cao, F.; Guo, S.; Jia, Y.; Zhang, D.; Liu, Z.; Wang, P.; Scudino, S.; Sun, J. Effects of Mg and Cu on microstructures and properties of spray-deposited Al-Zn-Mg-Cu alloys. *J. Alloys Compd.* **2017**, *719*, 89–96. [CrossRef]
23. Fang, H.; Luo, F.; Chen, K. Effect of intermetallic phases and recrystallization on the corrosion and fracture behavior of an Al-Zn-Mg-Cu-Zr-Yb-Cr alloy. *Mater. Sci. Eng. A* **2017**, *68*, 480–490. [CrossRef]
24. Liu, B.; Lei, Q.; Xie, L.; Wang, M.; Li, Z. Microstructure and mechanical properties of high product of strength and elongation Al-Zn-Mg-Cu-Zr alloys fabricated by spray deposition. *Mater. Des.* **2016**, *96*, 217–223. [CrossRef]
25. Guan, R.; Shen, Y.; Zhao, Z.; Wang, X. A high-strength, ductile Al-0.35Sc-0.2Zr alloy with good electrical conductivity strengthened by coherent nanosized-precipitates. *Mater. Sci. Technol.* **2017**, *33*, 215–223. [CrossRef]
26. Xu, Y.; Zhang, Z.; Gao, Z.; Bai, Y.; Zhao, P.; Mao, W. Effect of main elements(Zn, Mg and Cu) on the microstructure, castability and mechanical properties of 7xxx series aluminum alloys with Zr and Sc. *Mater. Charact.* **2021**, *182*, 458–464. [CrossRef]

27. Zhang, M.; Liu, T.; He, C.; Ding, J.; Liu, E.; Shi, C.; Li, J.; Zhao, N. Evolution of microstructure and properties of Al-Zn-Mg-Cu-Sc-Zr alloy during aging treatment. *J. Alloys Compd.* **2016**, *658*, 946–951. [CrossRef]
28. Huang, X.; Pan, Q.; Li, B.; Liu, Z.; Huang, Z.; Yin, Z. Microstructure, mechanical properties and stress corrosion cracking of Al-Zn-Mg-Zr alloy sheet with trace amount of Sc. *J. Alloys Compd.* **2015**, *650*, 805–820. [CrossRef]
29. Cvijović, Z.; Rakin, M.; Vratnica, M.; Cvijović, I. Microstructural dependence of fracture toughness in high-strength 7000 forging alloys. *Eng. Fract. Mech.* **2008**, *75*, 2115–2129. [CrossRef]
30. Rokni, M.R.; Zarei-Hanzaki, A.; Roostaei, A.A.; Abedi, H.R. An investigation into the hot deformation characteristics of 7075 aluminum alloy. *Mater. Des.* **2011**, *32*, 2339–2344. [CrossRef]